Applied Catalysis B: Environmental 203 (2017) 218–226

Contents lists available at ScienceDirect

Applied Catalysis B: Environmental

journal homepage: www.elsevier.com/locate/apcatb

Tail gas catalyzed N_2O decomposition over Fe-beta zeolite. On the promoting role of framework connected AlO_6 sites in the vicinity of Fe by controlled dealumination during exchange

Ignacio Melián-Cabrera[a,b,*], Ernst R.H. van Eck[c], Silvia Espinosa[b], Sandra Siles-Quesada[a], Lorena Falco[d], Arno P.M. Kentgens[c], Freek Kapteijn[b], Jacob A. Moulijn[b]

[a] European Bioenergy Research Institute (EBRI), School of Engineering and Applied Science, Aston University, Aston Triangle, Birmingham, B4 7ET, United Kingdom
[b] Delft University of Technology, Faculty of Applied Sciences, Catalysis Engineering, Chemical Engineering Department, Van der Maasweg 9, 2629 HZ Delft, The Netherlands
[c] Radboud University, Institute for Molecules and Materials, Heyendaalseweg 135, 6525 AJ, Nijmegen, The Netherlands
[d] Chemical Reaction Engineering, ENTEG, University of Groningen, Nijenborgh 4, 9747 AG Groningen, The Netherlands

ARTICLE INFO

Article history:
Received 27 June 2016
Received in revised form 1 October 2016
Accepted 8 October 2016
Available online 11 October 2016

Keywords:
N_2O decomposition
Fe catalysts
Zeolite beta
Catalyst stability
Environmental catalysis

ABSTRACT

A novel route to prepare highly active and stable N_2O decomposition catalysts is presented, based on Fe-exchanged beta zeolite. The procedure consists of liquid phase Fe(III) exchange at low pH. By varying the pH systematically from 3.5 to 0, using nitric acid during each Fe(III)-exchange procedure, the degree of dealumination was controlled, verified by ICP and NMR. Dealumination changes the presence of neighbouring octahedral Al sites of the Fe sites, improving the performance for this reaction. The so-obtained catalysts exhibit a remarkable enhancement in activity, for an optimal pH of 1. Further optimization by increasing the Fe content is possible. The optimal formulation showed good conversion levels, comparable to a benchmark Fe-ferrierite catalyst. The catalyst stability under tail gas conditions containing NO, O_2 and H_2O was excellent, without any appreciable activity decay during 70 h time on stream. Based on characterisation and data analysis from ICP, single pulse excitation NMR, MQ MAS NMR, N_2 physisorption, TPR(H_2) analysis and apparent activation energies, the improved catalytic performance is attributed to an increased concentration of active sites. Temperature programmed reduction experiments reveal significant changes in the Fe(III) reducibility pattern with the presence of two reduction peaks; tentatively attributed to the interaction of the Fe-oxo species with electron withdrawing extraframework AlO_6 species, causing a delayed reduction. A low-temperature peak is attributed to Fe-species exchanged on zeolitic AlO_4 sites, which are partially charged by the presence of the neighbouring extraframework AlO_6 sites. Improved mass transport phenomena due to acid leaching is ruled out. The increased activity is rationalized by an active site model, whose concentration increases by selectively washing out the distorted extraframework AlO_6 species under acidic (optimal) conditions, liberating active Fe species.
© 2016 Elsevier B.V. All rights reserved.

1. Introduction

Fe-zeolites have drawn considerable attention for their use in the decomposition of N_2O, a highly relevant process for the reduction of the greenhouse-gas industrial emissions. Low temperature N_2O decomposition in the tail gas of nitric acid facilities (*e.g.* UHDE process) [1] has been an active research area in the last decades [2–4]. Besides N_2O, the nitric acid plant exhaust lines contain gases such as O_2, NOx and H_2O that can hamper the intrinsic catalyst activity. Fe-containing ferrierite [5–10], ZSM-5 [3,11–18], beta zeolites [3,10,14,19–24] and TNU/IM-type zeolites [25] are the most active formulations. Fe-ferrierite appears to be the most active catalyst; the arrangement of Fe in the cavity of ferrierite produces a suitable interaction between two Fe cations. This results in a Fe-to-Fe distance of about 7 to 7.5 Å, which is comparable to the length of the N_2O molecule and the origin of the high turnover frequency of Fe-ferrierite; such an arrangement does not exist in beta or ZSM-5 [26,27]. This reaction has been reviewed recently in terms of

* Corresponding author at: European Bioenergy Research Institute (EBRI), School of Engineering and Applied Science, Aston University, Aston Triangle, Birmingham, B4 7ET, United Kingdom.
E-mail address: ignacio.cabrera.TUD@outlook.com (I. Melián-Cabrera).

http://dx.doi.org/10.1016/j.apcatb.2016.10.019
0926-3373/© 2016 Elsevier B.V. All rights reserved.

mechanistic studies based on spectroscopic, kinetic and molecular simulations [28].

For this application, Fe-zeolites can be prepared in a variety of ways. The most common routes are to introduce iron by post-synthetic liquid phase ion-exchange [3,5–10,15,16,18–24,26,27] also called 'wet ion-exchange route', chemical vapour deposition, also called 'solid ion-exchange' [12,13,17,18,21], or by hydrothermal synthesis [11,14].

Besides the preparation method, high-temperature treatments such as dehydroxylation and steaming, are key steps to enhance the intrinsic activity. Pérez-Ramírez et al. demonstrated for isomorphously Fe-substituted ZSM-5 [11,14] and beta [14] that steaming is crucial for creating the active species, characterized as extraframework Fe [29], resulting in an excellent N_2O-decomposition activity and stability. After steaming, "ex-lattice" Fe-sites in combination with Al, of the hydrothermally synthesized Fe containing ZSM-5, also display an enhanced performance for the N_2O mediated oxidation of benzene to phenol [30–32]. Application of a high-temperature treatment or steaming also promoted the performance of solid ion-exchanged Fe-ZSM-5 [17,33,34], giving rise to an increased N_2O decomposition rate. Pirngruber et al. reported that high temperature and steaming generally enhances the intrinsic activity of various kinds of Fe-prepared ZMS-5 and ZSM-12 [12], including hydrothermal [12], liquid phase- [18] and solid ion-exchange [12,18] routes.

Investigations of such treatments of other zeolite-based catalysts, such as Fe-containing ferrierite and beta, are barely found. In an elegant study on beta and ferrierite, Kaucký et al. [10] observed an increased N_2O conversion upon the formation of Al-Lewis sites neighbouring Fe-sites, as a result of dehydroxylation. For Fe-ferrierite the effect was more pronounced under pure N_2O, but it almost disappeared when NO was co-fed. Fe-beta zeolite behaved differently, showing the promoting effect in both pure N_2O and NO-containing feed. An electronic effect causing a faster recombination of oxygen atoms was proposed. Recently, Wang et al. reported on the promoting effect of extra-framework Al, added as $AlCl_3$, on the structure of Fe/ZSM-35 [35,36]; it was suggested that the addition of extraframework Al species is beneficial for the formation and reduction of binuclear active Fe sites bound to the extra-framework Al species.

In this work, a novel route to prepare Fe-based beta zeolite catalysts is presented, where the Al-speciation was tuned in order to verify if the presence of neighbouring extraframework AlO_6 sites enhances the performance for this reaction. The fraction and type of AlO_6 can be controlled by leaching using mineral acids in solution, according to well-established protocols for dealuminating zeolites [37,38]. The acid treatment was carried out during the liquid ion-exchange of Fe-cations by adjusting the pH systematically over a range from 3.5 to 0. The catalysts were tested in N_2O decomposition under tail gas conditions, accounting for the effect of H_2O, O_2 and NOx, to arrive at an optimal formulation for operation and stability. Physico-chemical characterizations allowed the interpretation of the observed performance and an active site model was proposed.

2. Experimental

2.1. Catalyst preparation

The catalysts were prepared by wet ion-exchange, contacting the powdery zeolite beta (Zeolyst CP-814E, NH_4-form) with a solution of ferric nitrate (Riedel-de-Haën) under continuous stirring at 353 K for 6 h. The pH was fixed for each exchange; for this a controlled amount of nitric acid (Merck) was added at the beginning of the exchange. The preparations range a pH from 0 to 3 with increments of 0.5. A reference experiment was carried out without the addition of nitric acid, where the final obtained pH was nearly ~3.5 (sample denoted as Fe(4.5)BEA-3.5). This pH is produced by the slurry solution containing the zeolite and the Fe salt precursor. The ion-exchange was performed for 20 h. The Fe target content was 0.5 wt.% and in some cases it was increased to 1 wt.% in an optimization study. The samples were dried overnight at 383 K and calcined at 823 K for 4 h at a heating rate of 2 K min^{-1}. The sample code is suffixed with the exchange pH and prefixed with the obtained Fe-content; for simplicity the Fe-content is expressed as *per mille* (*i.e.* 10× wt.% Fe). A reference benchmark catalyst with 1 *wt.%* Fe (nominal composition) was prepared by ion-exchange with a Ferrierite zeolite (Tosoh HSZ-720KOA, Si/Al = 9.2, K-FER). K-FER was exchanged twice (1.0 and 2.0 M NH_4NO_3 for 24 h at 80 °C), washed thoroughly after each exchange and dried. Fe ion-exchange was applied afterwards, followed by drying and calcination according to the procedure described above.

2.2. Activity tests

Activity tests were carried out in a six-flow reactor set-up using 50 mg of catalyst particles (125–250 μm) [39]. The catalysts were tested in N_2O/He (4.5 mbar N_2O) at a total pressure of 3 bar absolute and a space time of $W/F^o(N_2O)$ 900 kg s mol^{-1} (where W is the catalyst mass and $F^o(N_2O)$ the molar flow of N_2O in the feed). The reactor outlet was analyzed by gas chromatography. The chromatograph (Chrompack CP 9001) was equipped with a Poraplot Q column (for N_2O and N_2/O_2 separation) and a Molsieve 5A column (for N_2 and O_2). Before reaction, the catalysts were pretreated in a flow of He at 673 K for 1 h, and cooled down in the same gas to the starting reaction temperature. After 1 h on-stream steady state was considered to be reached, since the composition of the product flows were constant.

The catalyst performance was also tested under nitric acid-based tail gas conditions with the following composition: 4.5 mbar N_2O, 0.6 mbar NO, 15 mbar H_2O and 75 mbar O_2, maintaining the same space time $W/F^o(N_2O)$ of 900 kg s mol^{-1} at 3 bar of total pressure. Stability tests were carried out under these conditions at 723 K for 70 h time on stream.

The first order rate constant per weight basis (k_w^{obs}, mol Pa^{-1} kg^{-1} min^{-1}) and the apparent activation energies (E^{app}, kJ mol^{-1}) were calculated assuming plug flow and first order kinetics in N_2O [40–42], using the following relations:

$$k_w^{obs} = \frac{F(N_2O)_o}{W_{cat} \cdot p(N_2O)_o} \ln\left(\frac{1}{1-x}\right) \quad (1)$$

$$E^{app} = -\frac{\partial(\ln k_w^{obs})}{\partial\left(1/T\right)} R \quad (2)$$

Experimental turnover frequencies (*TOF, min*$^{-1}$) were determined with this simplified equation:

$$TOF = \frac{x \cdot F\,N_2O_o \cdot A_r^{Fe}}{W_{cat} \cdot [Fe]} \quad (3)$$

In these relations x is the N_2O conversion (−), $F(N_2O)_o$ is the N_2O molar feed flow (mol min^{-1}), $p(N_2O)_o$ is the N_2O partial pressure (Pa), W_{cat} is the amount of catalyst (g), [Fe] is the Fe concentration (g_{Fe}/g_{cat}) determined by ICP, A_r^{Fe} is the molar mass of Fe (g/mol), T is the temperature (K) and R is the universal constant (8.314 J mol^{-1} K^{-1}). The activation energy was determined from an Arrhenius plot.

2.3. Characterization

Elemental analysis (Si, Al and Fe) of the dissolved catalysts was obtained by ICP-OES (Perkin-Elmer Optima 3000DV). Temperature-

programmed reduction with H_2 was carried out in a Micromeritics TPD/TPR 2900 apparatus, using a high purity mixture of 10 vol.% H_2/Ar. The samples were pretreated in He at 423 K for 1 h. After cooling down, they were flushed with the reduction mixture at room temperature until the baseline got stabilized, and the temperature program was started at a ramping rate of 10 K min^{-1}. After passing through a cold trap (isopropanol/liquid nitrogen) to retain the produced water, the gas from the reactor outlet was monitored by a TCD detector.

Nitrogen physisorption analyses (77 K) were carried out in a Micromeritics ASAP 2420. The samples were degassed in vacuum at 623 K for 10 h. The BET area (S_{BET}) was calculated using the standard method [43]. The single point pore volume (V_T) was estimated from the amount of gas adsorbed at a relative pressure of ~0.98 in the desorption branch. The micropore volume (V_{MICRO}) and surface area (S_{MICRO}) were calculated from the ***t***-plot method; the mesoporous surface area (S_{MESO}) is calculated as: $S_{MESO} = S_{BET} - S_{MICRO}$.

The XRD pattern of the as-received BEA zeolite was recorded in a Bruker-Nonius D-5005 diffractometer equipped with a graphite monochromator, over a range of 2θ angle from 5 to 50°. The crystalline phase was identified using the Joint Committee on Powder Diffraction Standards (JCPDS) file no. 48-0074 for beta zeolite, as given in Fig. S-1.

Quantitative, high-resolution Single Pulse Excitation (SPE) ^{27}Al MAS NMR spectra were measured on a Varian 600 MHz spectrometer using 1.6 mm PENCIL design probe, resonant for ^{27}Al at 156.337 MHz. Spectra were acquired under magic angle spinning at 32 kHz. Special care was taken in order to obtain quantitative spectra from quadrupolar nuclei: using short pulses (3 μs) at a low rf field strength (8.3 kHz) and a recycle delay well outside 5 times T_1 (<20 ms) ensured this. A small contribution from an Al background signal present in the MAS rotors was corrected for, and signal intensities were scaled for sample weights. The amounts of the different Al species can be determined by integrating the spectra between the regions of AlO_6 [−50, 10 ppm], AlO_5 [10–30 ppm] and AlO_4 [30–100] ppm. The ^{27}Al chemical shift was referenced to $Al(NO_3)_3$.

The ^{27}Al MQ MAS NMR experiments were performed on a Chemagnetics 600 MHz NMR spectrometer at a magnetic field strength of 14.1 T with an aluminium Larmor frequency of 156.34 MHz. Further details about these measurements can be found in van Eck et al. [44].

3. Results

A series of catalysts were prepared aiming at an iron content of 0.5 wt.%. Elemental analysis proves that except for the catalyst prepared at pH = 0, the achieved Fe content was close to the target value, with a slight decrease for samples prepared at decreasing pH (Table 1). The catalyst prepared at pH = 0 contained hardly any Fe (0.01 wt.%).

The Si/Al ratio as determined from ICP was examined to gain a better understanding of the pH effect during the exchange (Table 1). The Si/Al for the as-received zeolite was 11, close to the commercial specifications (12.5). The Si/Al ratio remains constant after the ion-exchange for samples prepared at pH = 2 and higher. Below this pH, the Si/Al ratio increases due to dealumination under these harsher acidic conditions [37,38], ranging from 13 to 24. A step increase is found for pH = 0 with a Si/Al ratio of 93.

Verifying if the zeolite exchange capacity may be modified by dealumination is crucial for the data interpretation. The zeolite exchange capacity can be estimated for the observed Si/Al ratios, assuming a theoretical exchange ratio of Al/Fe = 3, since one Al atom provides one exchange site and Ferric ions were employed. This is indeed global since the Al framework sites will not be so close together to achieve this; only for extraframework Al this does apply reasonably. Assuming that the Fe species are hydroxylated, less Al exchange sites are required and the exchange capacity would be higher. The maximum Fe exchange capacities were calculated in this way (Al:Fe = 3:1) and compiled in Table 1 (given as Fe^{max}). The values in parenthesis (6th column) are the achieved exchange (%), relative to the maximum Fe^{max} loading capacity. In general, the increase of the Si/Al ratio does not limit the exchange capacity for the applied 0.5 wt.% target Fe concentration. In most cases, the theoretical maximum Fe-loading ranges between 1.2 to 2.7 wt.%, and the achieved exchange levels vary between 15 and 31%. The limiting case was observed for the pH = 0 where a maximum loading of 0.3 wt.% can be exchanged. The low Fe amount achieved in that sample (0.01 wt.%) is attributed to a competition between aqueous H^+ and Fe^{3+} for exchange on the residual Brønsted sites. Such a competition also exists for the other catalysts since the observed Fe loading was always slightly lower than the target 0.5 wt.%. Thus, the Fe loading was generally close to the target value with a slight decrease with lowering pH, except for pH = 0 where the Fe loading was significantly hindered due to extensive dealumination (implying reduced exchange sites) and especially to the H^+ exchange competition. Note that the Fe loading (0.01 wt.%) is lower than that of the starting zeolite (0.02 wt.%), which implies a 'negative' exchange as shown in Table 1. The negative value is an artefact as consequence of the leaching of Fe impurities contained in the starting native zeolite beta at pH = 0.

Fig. S-1 contains the XRD patterns of the catalyst series, for samples down to pH = 1. All the patterns are very similar, with reflections of a well-defined beta zeolite structure. Therefore, the leaching conditions up to the (optimal) pH = 1 does not alter the zeolite structure. The variation in the d-spacing is an instrumental issue due to the sample holder. Fig. S-1 also includes an optimized material, denoted Fe(7.1)BEA-1, as discussed later, that keeps the beta zeolite structure as well.

Solid-state ^{27}Al MAS NMR was applied to investigate the state of the Al coordination. Fig. 1 shows the single pulse excitation (SPE) 1D spectra of the relevant catalysts. The spectra display an intense resonance at *ca.* 60 ppm due to tetrahedrally coordinated Al (AlO_4), characteristic of zeolite framework Al species [45] (sketched in Fig. 2a); and a second broad resonance ascribed to octahedrally coordinated Al (AlO_6) in the region around 0 ppm [45]. In the octahedral region, two contributions are visible with a sharp resonance centred at −1 ppm, overlapping with a broad contribution ranging from ~−40 to 10 ppm. It has been proposed [46–48] that the sharp octahedral peak is ascribed to framework connected octahedral Al (Fig. 2b), while the broader resonance is related to Al that has lost the connection to the framework oxygen (Fig. 2c), though part of that distorted octahedral Al can be reconverted into framework AlO_4 [47]. The asymmetry of the main resonance at around 50 ppm indicates the presence of penta-coordinated Al (AlO_5) as well [45,46]. Fig. S-2 shows the MAS NMR spectra of the as-received and calcined beta zeolites. The as-received sample spectrum is mainly composed of AlO_4 (>97%) while the calcined sample also contains substantial amount of AlO_5 (7%) and AlO_6 (29%). This comparison demonstrates that the calcination process causes the development of AlO_5 and AlO_6.

Fig. 3 compiles the relative composition after quantitative analysis of the spectra from Fig. 1 and Fig. S-2, normalized to the intensity of the as-received beta zeolite. The narrow AlO_4 resonance seems to increase from the sample **A** Fe(4.5)BEA-3.5 up to **C** Fe(4.2)BEA-2 and then the intensity is reduced at **D** Fe(4.2)BEA-1.5 and **E** Fe(4.0)BEA-1. The total amount of Al observed by NMR (per gram of sample) decreases at low pH (samples **D** and **E**, Fig. 3) due to the dealumination, which is consistent with the observed Si/Al determined by ICP – for the sake of clarity the Si/Al values are included in Fig. 3 (*bottom*). The broad AlO_6, and AlO_5, decrease monoton-

Table 1
Catalyst codes, exchange conditions and elemental analyses (ICP).

Entry	Catalyst code	pH (−)[a]	Si/Al (mol)	Fe^{max} (wt. %)[b]	Fe^{ICP} (wt. %)[c,d]
1	BEA	*as-received*[e]	11.0	2.55	0.0224 (0)
2	Fe(4.5)BEA-3.5	3.5	10.3	2.71	0.45 (16)
3	Fe(5.2)BEA-2.5	2.5	10.5	2.66	0.52 (18)
4	Fe(4.2)BEA-2	2.0	10.9	2.58	0.42 (15)
5	Fe(4.2)BEA-1.5	1.5	13.0	2.19	0.42 (18)
6	Fe(4.0)BEA-1	1.0	24.0	1.23	0.40 (31)
7	Fe(0.1)BEA-0	0.0	93.0	0.33	0.01 (−4)
8	Fe(7.1)BEA-1	1.0	28.1	1.06	0.71 (63)
9	Fe(9.5)FER	–	9.4	2.94	0.95 (32)[f]
10	BEA−1[g]	1.0	22.5	1.31	0.0205 (∼0)

[a] Applied pH during Fe exchange.
[b] Maximum Fe loading as wt.% assuming 3Al/Fe for the observed Si/Al ratio.
[c] Target Fe loading: 0.5 wt.% Fe, except for entry 8, which was 1 wt.%.
[d] In parenthesis, Fe exchange (%) = $[Fe^{sample} - Fe^{BEA}]/Fe^{max} \times 100$, where Fe^{BEA} corresponds to the Fe loading for the parent zeolite beta, given in entry 1.
[e] Thermally treated at 823 K.
[f] Calculated based on an Fe content in raw FER of 0.010 wt.%.
[g] As-received zeolite treated at pH = 1 and calcined (thus, identical process as Fe(4.0)BEA-1 without Fe addition).

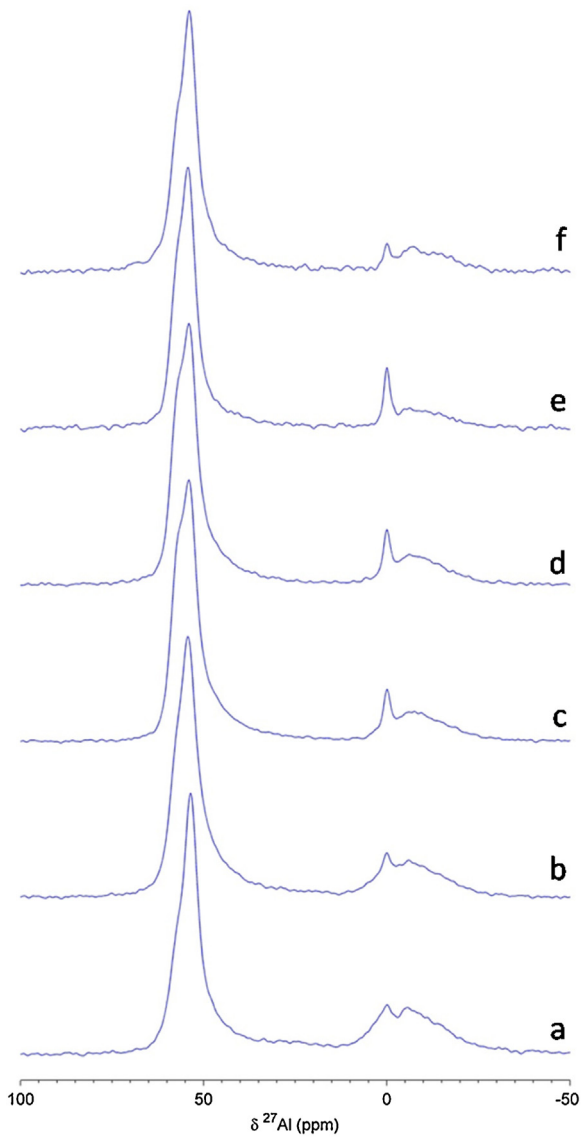

Fig. 1. Quantitative, high-resolution ^{27}Al MAS NMR spectra: (a) Fe(4.5)BEA-3.5; (b) Fe(5.2)BEA-2.5; (c) Fe(4.2)BEA-2; (d) Fe(4.2)BEA-1.5; (e) Fe(4.0)BEA-1; (f) Fe(7.1)BEA-1.

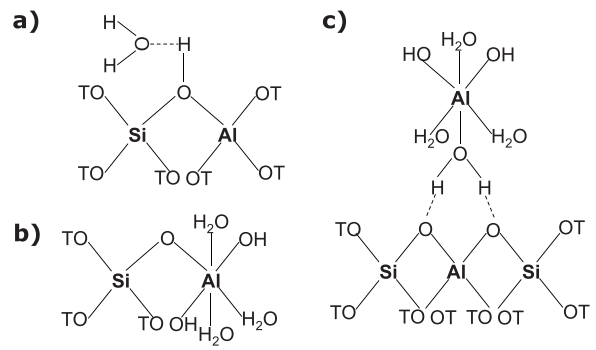

Fig. 2. Proposed Al species present in the beta zeolites, in the hydrated forms: (a) framework AlO_4, (b) framework connected AlO_6 with at least one connected oxygen atom, represented as $[Al(OH)_2(OT)(H_2O)_3]$, (c) extraframework AlO_6, defined as $[Al(OH)_3(H_2O)_3]$ connected via water, though polynuclear species denoted as $Al_nOH_{2n}^+$ are also possible.

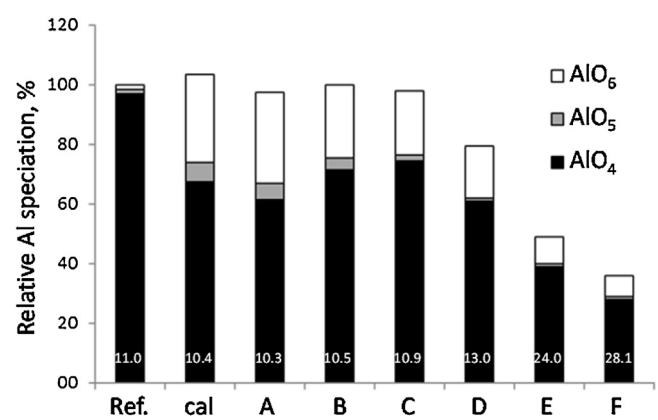

Fig. 3. Aluminum speciation derived from ^{27}Al MAS NMR spectra given as percentage with respect to the reference sample, the as-received NH_4-form beta zeolite. Codes: (Ref) As-received NH_4-form beta zeolite; (cal) calcined beta; (A) Fe(4.5)BEA-3.5; (B) Fe(5.2)BEA-2.5; (C) Fe(4.2)BEA-2; (D) Fe(4.2)BEA-1.5; (E) Fe(4.0)BEA-1; (F) Fe(7.1)BEA-1. The Si/Al ratio determined by ICP has been added for the sake of clarity. Spectra for the as-received beta (denoted as 'ref') and calcined (A) can be found in Fig. S-2, in the Supporting information.

ically, indicating that under the acid conditions these species are preferentially washed out. Sample **F** (Figs. 1 and 3) is made for optimization doubling the Fe loading, which will be discussed later in terms of performance. Its NMR features follow the trend discussed for the 0.5 wt.% series: a reduced total resonant Al (due to dealumination mainly) and lower fraction of AlO_6 and AlO_5 due to selective

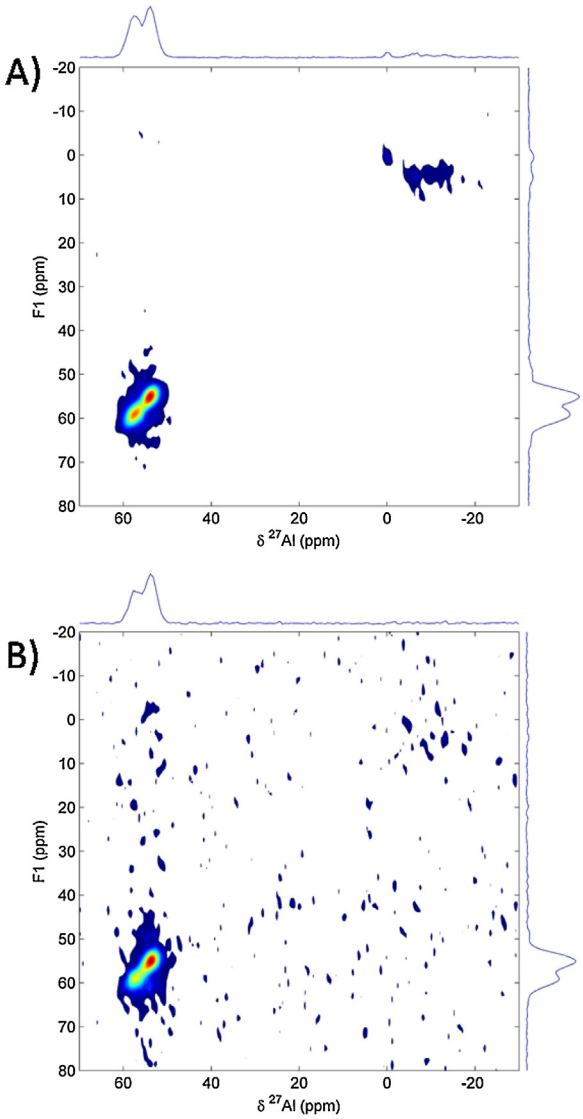

Fig. 4. ^{27}Al MQ MAS NMR for the catalysts: (a) Fe(5.2)BEA-2.5; (b) Fe(7.1)BEA-1.

leaching. A difference is the lower intensity of the framework connected AlO_6 species, compared to the equal pH counterpart, *cf.* samples **E** and **F** (Fig. 1). This reduction in intensity can be associated to the preferential interaction with Fe, which is in this case double than for sample **E**. The major observations by SPE NMR are that AlO_5 and AlO_6 are selectively washed out from the structure upon decreasing pH to 2; at pH < 2, AlO_4 is also leached out. In general, the remaining AlO_6 becomes preferentially well-defined framework connected octahedral Al (sharp resonance at −1 ppm), that appears to interact with Fe – this is seen when doubling the Fe loading (*cf.* SPE patterns for samples **E** and **F**, Fig. 1). A second major point is the agreement of the ICP results with the observed total resonant Al signal.

^{27}Al MQ MAS NMR experiments were carried out to evaluate the status of the AlO_4 in more detail. Fig. 4 shows the MQ MAS spectra for two representative catalysts, Fe(5.2)BEA-2.5 and Fe(7.1)BEA-1, prepared at pH = 2.5 and 1. No significant distinctions were found at the tetrahedral species; both show two types of framework tetrahedral Al, consistent with Kentgens and co-workers [47]. The lack of AlO_6 speciation for the Fe(7.1)BEA-1 sample in the MQ MAS spectra is noteworthy (Fig. 4b). This might be related to: (1) the differences in the material's hydration that is known to lead to a dispersion in its chemical shift, (2) to the quadrupole interaction, which broadens its line width in the hydrated state [49], (3) as this material contains double Fe loading (vide infra) the paramagnetic effect of Fe may suppress the Al signal, hence part of the Al might not be visible in the MQ MAS NMR spectrum as a result of the paramagnetic nature of the iron species [31,33]. In fact Al can be partly exchanged with Fe(III) species according to the reversibility model demonstrated by Kentgens et al. [47] that will enhance this effect.

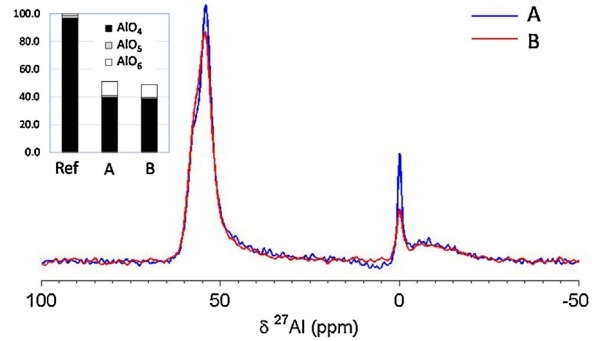

Fig. 5. Quantitative, high-resolution ^{27}Al MAS NMR normalized spectra: (a) Fe(4.0)BEA-1 and (b) BEA-1. The inset represents the Al speciation percentage in comparison with the as-received BEA (denoted as 'Ref'; spectrum can be found in Fig. S-2).

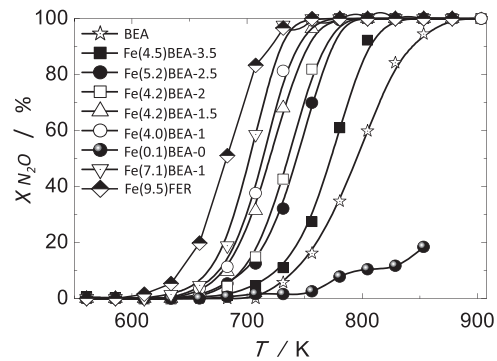

Fig. 6. Performance of the Fe-BEA catalysts prepared by wet ion exchange at various pH. Catalyst codes can be found in Table 1. Reaction conditions: 4.5 mbar N_2O in He at 3 bara total pressure and $W/F^0(N_2O)$ of *ca.* 900 kg s mol^{-1}.

The effect of the paramagnetic nature of Fe leads to the question whether all distorted non-framework Al disappears upon leaching, or becomes partly invisible due to interaction with the added Fe. In order to answer to this question, the spectra of a control sample were compared to those of Fe(4.0)BEA-1 (Fig. 5). The control sample is the native zeolite that was treated at pH = 1 without any Fe(III)-exchange, and calcined. Hence it has undergone a similar treatment as Fe(4.0)BEA-1 except for the Fe addition step, so the effect of Fe can be directly compared. The spectra of both materials are very similar, formed by AlO_4, AlO_5 and AlO_6. Comparison indicates that the intensity of the AlO_4 and framework connected AlO_6 are reduced, indicating that these are Al centers of preferential interaction with Fe. The distorted non-framework Al content is low for both materials, as compared to the calcined counterpart (Fig. S-2), but importantly it is nearly equal for both samples. Hence Fe does not interact with these domains. It is then concluded that the acid leaching gives rise to the preferential removal of non-framework Al and the added Fe interacts/exchanges preferentially with AlO_4 and framework-connected AlO_6.

The catalysts were tested in the N_2O decomposition. Fig. 6 shows the N_2O conversion as a function of the reaction temperature ranging between 500 and 900 K. For all the catalysts, N_2O was decomposed stoichiometrically into nitrogen and oxygen. The light-off temperature was observed around 650 K, while

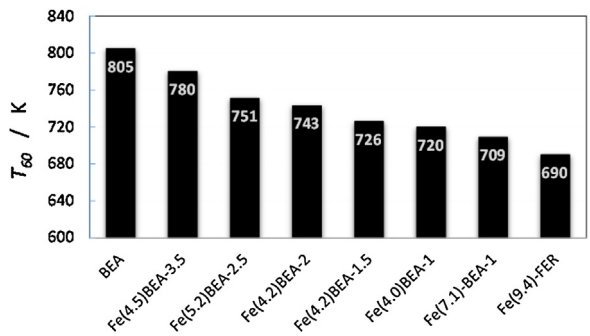

Fig. 7. Temperature (K) for 60% N_2O conversion (T_{60}) for the studied catalysts, derived from Fig. 6.

the conversion increased at different rates for the different catalysts. The parent zeolite (BEA, in Fig. 6) was also active in the reaction, attributed to the presence of Fe impurities from the zeolite manufacturing process [50,51], which was ~224 ppm (Table 1). When compared to the reference catalyst, *i.e.* Fe(4.5)BEA-3.5, the catalysts' performance increased significantly with decreasing pH during exchange. This can be expressed as an increased conversion at isothermal conditions, or as a lowering of the reaction temperature at isoconversion. The latter is illustrated in Fig. 7, where the temperature to accomplish 60% N_2O conversion (T_{60}) is plotted as a function of the catalysts' exchange pH. A reduction of *ca* 70 K was found in the series, between the reference and the optimal Fe(4.0)BEA-1. The poor performance of Fe(0.1)BEA-0 is consistent with the low Fe loading (0.01 wt.%, a lower residual Fe content due to leaching, as discussed above). Thus the optimal exchange pH was found to be 1.

An additional optimization step was carried out by preparing a catalyst at pH of 1, aiming at an iron loading of 1 wt.%. Experimentally 0.71 wt.% was found, consistent with the same trend in the 0.5 wt.%-series, since the loading is nearly double that of the Fe(4.0)BEA-1 (0.4 wt.%). This Fe(7.1)BEA-1 catalyst exhibited a significant improved performance with a reduction of the T_{60} down to 709 K, which is nearly 100 K lower than the reference catalyst (Figs. 6 and 7). A prepared benchmark Fe-ferrierite catalyst, Fe(9.5)FER, containing *ca.* 1% Fe, tested under identical reaction conditions, is the most active, but the activity of the optimal Fe(7.1)BEA-1 is close to it (Fig. 6). The comparison in Fig. 7 indicates that its T_{60} is only 19 °C higher than the ferrierite based catalyst.

This optimal Fe(7.1)BEA-1 catalyst was further evaluated under nitric acid tail gas conditions, which involves O_2, NO and H_2O, in addition to N_2O (Fig. 8, *top*). Clearly, the combined effect of the tail gas components ($NO + H_2O + O_2$) has no significant impact on the catalyst performance compared with pure N_2O/He. This behaviour can be explained by former investigations of the individual components effect [7,11,52]. It was demonstrated that NO has a promoting effect, by enhancing the removal of deposited oxygen species [53]; water negatively affects the activity by hydroxylation of the active sites – some mechanistic insights have been demonstrated for water, such as blocking binuclear Fe sites [54], or modification of the apparent activation energy and pre-exponential factor [55]. O_2 has no or little influence. The overall effect of the tail gas components, compared to pure N_2O/He, has been in general positive (Fe-ZSM-5) [11,52] or neutral (Fe-ferrierite) [7] to the performance. This study reveals that beta behaves slightly positive under tail gas conditions (Fig. 8, top).

The catalyst stability evaluated at 723 K using the complete tail gas mixture (Fig. 8, bottom) indicated no apparent activity loss after 70 h. Hence the presented catalyst preparation route yields a competitive Fe-based beta zeolite catalyst for N_2O decomposition in terms of overall performance, with comparable conversion levels as a state-of-the-art reference catalyst (Fe-ferrierite) and good stability under industrially relevant conditions.

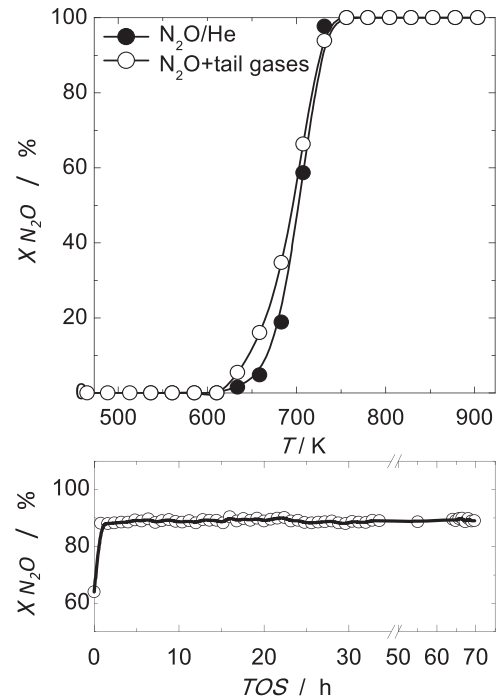

Fig. 8. (Top) N_2O conversion for the Fe(7.1)BEA-1 catalyst for a N_2O/He mixture: 4.5 mbar N_2O in He at 3 bara total pressure and $W/F^0(N_2O) \approx 900$ kg s mol^{-1} and with the addition of tail gas components: 0.6 mbar NO, 15 mbar H_2O and 75 mbar O_2, maintaining the same space time. (Bottom) N_2O conversion at 723 K as a function of time on stream (*TOS*) for the same catalyst under tail gas conditions: 4.5 mbar N_2O, 0.6 mbar NO, 15 mbar H_2O and 75 mbar O_2 in He at 3 bara total pressure and $W/F^0(N_2O) \approx 900$ kg s mol^{-1}.

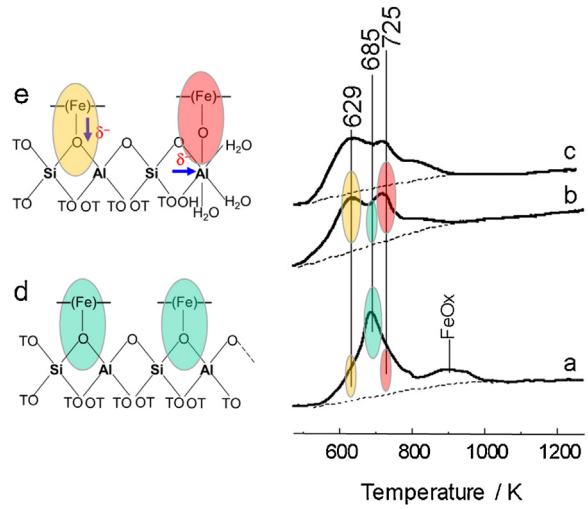

Fig. 9. Suggested Fe-sites assignments based on NMR results. (Right) Temperature-programmed reduction profiles for: (a) Fe(5.2)BEA-2.5; (b) Fe(4.0)BEA-1 and (c) Fe(7.1)-BEA-1; Left) plausible Fe-sites: (d) Fe-species exchanged in pristine framework AlO_4 and (e) Fe-species exchanged on AlO_4 that are in interaction with framework-connected AlO_6. The colour in the TPR profiles indicate qualitatively the proportion of each site, the sites are defined on the left side (d and e).

Temperature programmed reduction (TPR) experiments provide evidence on the interaction between Fe and Al species in the optimal catalysts. The TPR profiles of the optimal catalysts (Fig. 9, patterns b and c) contain two reduction peaks, centred at 629 and 725 K, which are typically ascribed to Fe exchanged species [6,16]; no FeOx was observed. For comparison the Fe(5.2)BEA-2.5 cata-

Table 2
Texture parameters of relevant catalysts derived from N_2 physisorption at 77 K.

Material	V_T (cm^3/g)	V_{MICRO} [a] (cm^3/g)	S_{BET} (m^2/g)	S_{MICRO} (m^2/g)	S_{MESO} (m^2/g)
BEA	0.972	0.177 (0.795)	585	365	220
Fe(7.1)BEA-1	0.995	0.154 (0.841)	595	320	275

[a] Value in parenthesis is the external pore volume as: $V_T - V_{MICRO}$.

lyst, with a low level of dealumination, has a small contribution of inactive FeOx, visible at 900 K (Fig. 9, pattern a).

The TPR interpretation is based on the NMR findings, that showed the preferential interaction between Fe and framework AlO_4 and with framework connected AlO_6 (Fig. 5). The low-temperature TPR peaks in Fig. 9 are attributed to Fe-*oxo* species formed by at least two Fe sites (dinuclear oxygen bridged iron sites are often proposed) on the AlO_4 sites, which are found to be responsible of the high turnover rate for N_2O decomposition [26,54–56]. The position of the first reduction peak at 629 K is ~55 K lower than the main reduction in the Fe(5.2)BEA-2.5. This shift to lower temperatures can be attributed to an electronic effect due to the electron withdrawing capacity of AlO_6 that makes the AlO_4 sites positively charged, leading to an easier reduction of the Fe(III) species. The reduction at 725 K, which is 40 K shifted to higher temperatures, is ascribed to Fe species exchanged/adsorbed on the electron withdrawing AlO_6 species that are negatively charged, that impede their reduction. Note that the reference catalyst, Fe(5.2)BEA-2.5, displays shoulders at 629 and 725 K that can be interpreted to the presence of such Fe-species in interaction with framework connected AlO_6.

4. Discussion

The increasing performance of the catalyst series in N_2O decomposition can be discussed in various terms, such as metal loading and speciation; the latter may involve new species, and this can be detected by the apparent activation energy, or an increase of the active/selective species during the preparation method. The increase of the active/selective species are generally more difficult to demonstrate and normally require a multi-technique approach and theoretical tools.

Zhang et al. [28] rationalized the effect of the pH during the metal ion exchange; the effect has been typically studied by the consequences of the different types of metal species on the performance. The effect of the Al speciation of zeolite beta structures, in combination with metal species, has been barely investigated [57].

The above results clearly indicate that decreasing exchange pH, the performance was enhanced significantly. Such an effect cannot be explained by differences in the Fe loading, since the catalyst series, entries 2–6 (Table 1), has nearly the same Fe loading. Thus a clear pH-related effect takes place. The Si/Al ratio and NMR characterization indicated that dealumination occurs. For the optimal catalyst, pH = 1 (Fe(7.1)BEA-1), dealumination occurs but it is not excessive (Si/Al increased by a factor 2.6) while AlO_6 species with some kind of framework connection (resonance at −1 ppm, Fig. 1) become cleaned from other surrounding unconnected, distorted extraframework AlO_6 species. Hence the presence of isolated, framework connected AlO_6 could be essential for the observed increased activity.

Fig. 9e shows a model representing the electronic effect induced on the Fe sites. The electron density is partially displaced to the electron withdrawing AlO_6 sites, that are negatively charged. This affects the interaction with the Fe species. The sites in interaction with the positively charged AlO_4 are reduced easier (peak at 629 K), while those Fe sites interacting with the negatively charged framework connected AlO_6 are polarized and more difficult to be reduced (peak at 725 K, and higher temperature broad contribution). These results are consistent with Arnoldy and Moulijn [58] who showed that the reducibility of Co-ions of $CoAl_2O_4$ is strongly decreased by the presence of AlO species. This is attributed to an increased polarization of the Co-O bonds, decreasing their reducibility.

Table 3
Apparent activation energies (E^{app}) and *TOFs* (at 730 K) for direct N_2O decomposition.

Entry	Catalyst	E^{app} (kJ mol^{-1})	*TOF* (10^{-1} min^{-1})
1	Fe(4.5)BEA-3.5	191 ± 6	1.0
2	Fe(5.2)BEA-2.5	205 ± 8	2.4
3	Fe(4.2)BEA-2	216 ± 14	3.8
4	Fe(4.2)BEA-1.5	211 ± 4	5.9
5	Fe(4.0)BEA-1	214 ± 4	7.4
6	Fe(7.1)BEA-1	220 ± 11	5.0
7	Fe(9.5)FER	164 ± 6	3.8

Wang et al. [35,36], claimed binuclear Fe sites stabilized by extra-framework Al in Fe/ZSM-35 to have superior performance. This seems to be in line with a previous study [7], where the effect of the zeolite matrix to host Fe for N_2O decomposition was investigated; it was concluded that the most reducible Fe species, detected by H_2-TPR, dominated the N_2O decomposition performance. Three effects were further investigated to shed light on the improved performance: mass transport limitations, the energetics and number/concentration of active species.

One possible effect is that the dealumination removes extraframework species, making the available exchanged Fe species more accessible to the reactants. Texture analysis of the optimal catalysts (Table 2) reveals a significant increase of the mesoporous surface area, of about 26%, while the BET surface area barely increases (2%). The micropore volume is slightly reduced and converted into mesoporosity. Thus, this increased mesoporous surface area can also have an influence on the performance.

A lower apparent activation energy could be indicative of possible mass transport limitations. The similar apparent activation energies do not indicate mass transport limitations for the reference material, Fe(4.5)BEA-3.5, nor for the pH treated counterparts (Table 3). The obtained values are high, in the order of magnitude for reported Fe-containing zeolites [42,56]. Under internal diffusion control, the apparent activation energies would be much lower, in the order of half of the true activation energy, and zero when external mass transfer occurs [39]. Therefore, since there are no mass transfer related limitations, the higher activity indicates an increase in the amount of active sites. This is confirmed by the experimental *TOF* values (Table 3), where a clear trend can be seen. It increases from 0.10 min^{-1} up to a maximum of 0.74 min^{-1} at the optimal pH = 1 in line with the observed conversion curves. When the Fe concentration is doubled at this pH, the *TOF* is reduced by 30%. Thus not all the extra added Fe are active and perhaps even blocking part of the active Fe species. Thus, the combination of apparent activation energy and *TOF* calculations prove that a higher quantity of active species are present. It is noteworthy that the optimal catalyst has a *TOF* value that is nearly double that of the benchmark Fe-FER.

The oxygen removal is in a kinetic sense the rate determining step, so if oxygen removal is easier, then one would see that in an energy effect. As this is not the case, the interpretation points at the increase of active sites. TPR experiments indicate easily reducible species, but strictly speaking in H_2-TPR the hydrogen must be dis-

sociated, so this may not resemble the ease of oxygen removal, key for N_2O decomposition. Nevertheless, having more active sites also reduction with H_2 may occur earlier and the reduced sites may accelerate the dissociation and further reduction. Indirectly, TPR shows a correlation between the species reduced at low temperature and the N_2O decomposition activity in the series. Therefore it seems that the enhanced activity is related to a higher concentration of the active Fe sites. The fact that the apparent activation energy of N_2O decomposition is not changed, in combination with the interpretation above of the TPR profiles, point out that the activity of the reference catalyst originates from species that reduce at 629 K (a shoulder at the leading edge in its TPR pattern), thus only a small fraction of the Fe loading.

The overall interpretation of this study with beta zeolite is that the acidic conditions during Fe exchange help to change the Al speciation, cleaning the sample from non-framework connected AlO_6, and inducing an interaction between Fe and the framework connected AlO_6 and AlO_4, a key configuration relevant for the activity improvement. The schematic model of the active sites is represented in Fig. 9e. Such sites may already be inactively present in the reference catalyst but the removal of the undesirable AlO_6, liberates these, thereby increasing the concentration of active sites, in line with the increasing reduction peak at 629 K, representing the most active site. This is further elaborated in Fig. 9 that combines the TPR profiles with our assignment of the Fe sites. The reference catalyst contains mostly Fe-species exchanged at pristine framework AlO_4 (sites represented in Fig. 9d). In the optimal catalyst (Fig. 9b), these species may also be present but the majority are Fe-species exchanged at AlO_4 and in interaction with framework-connected AlO_6 (both sites are represented in Fig. 9e).

In terms of the stability, the optimal catalyst in the complete tail gas mixture behave superbly without any apparent activity decay in the 70 h test. A former study by Pieterse et al. [3] reported also about the good stability of Fe-beta prepared by wet-ion exchange in a conventional manner, albeit exhibiting a lower activity in combination with a higher Fe loading.

5. Conclusions

The performance of Fe-based zeolite beta catalysts, for N_2O decomposition, can be improved through the preparation method, by Fe(III) exchange at controlled and low pH conditions. A systematic study for the studied beta zeolite (CP814E) shows that a pH of 1 was optimal for the N_2O decomposition reaction, with a significant activity increase. At those conditions, Fe(III) exchange is not competing with H^+ and the zeolite dealumination is not too extensive, leaving enough Al(III) sites available for exchange with a preferential speciation. Further optimization by increasing the Fe loading at the optimal pH led to a very active catalyst, comparable to the benchmark Fe-Ferrierite, and it is stable under tail-gas conditions without any appreciable activity decay for 70 h.

Characterisation studies show dealumination with the predominance of AlO_4, well-defined framework-connected AlO_6 species, and the nearly complete removal of AlO_5 and non-connected distorted extraframework AlO_6. TPR indicates changes in the Fe(III) reducibility pattern due to an electronic interaction promoted by framework connected AlO_6 species. Effects of mass transport (limitations) and energetics were ruled out as being playing a role. The combination of apparent activation energy, TPR and *TOF* values, show that in the optimal catalyst a higher quantity of active species are present. The improvement in performance was then interpreted by an increased number of active species, which become more abundant when removing the distorted extraframework AlO_6.

Acknowledgements

Financial support for this research from NOVEM (Ministry of the Environment of The Netherlands) is gratefully acknowledged. IM-C thanks the *European Commission (Marie Curie Individual Fellowship, HPMF-CT-2002-01873)* for a post-doctoral fellowship. Support of NWO for the "Solid State NMR facility for Advanced Materials Science" is gratefully acknowledged. S.S-Q thanks the *European Commission* for an Erasmus+ grant.

Appendix A. Supplementary data

Supplementary data associated with this article can be found, in the online version, at http://dx.doi.org/10.1016/j.apcatb.2016.10.019.

References

[1] URL: https://www.thyssenkrupp.com/en/produkte/envinox.html (accessed 30.03.15).
[2] J. Pérez-Ramírez, F. Kapteijn, K. Schöffel, J.A. Moulijn, Appl. Catal. B: Environ. 44 (2003) 117–151.
[3] J.A.Z. Pieterse, S. Booneveld, R. v/d Brink, Appl. Catal. B: Environ. 51 (2004) 215–228.
[4] C. Perbandt, V. Bacher, M. Groves, M. Schwefer, R. Siefert, T. Turek, Chem. Ing. Tech. 85 (2013) 705–709.
[5] B. Neveu, C. Hamon, K. Malefant, French Patent WO 99/34901.
[6] A. Guzmán-Vargas, G. Delahay, B. Coq, Appl. Catal. B: Environ. 42 (2003) 369–379.
[7] I. Melián-Cabrera, C. Mentruit, J.A.Z. Pieterse, R.W. van den Brink, G. Mul, F. Kapteijn, J.A. Moulijn, Catal. Commun. 6 (2005) 301–305.
[8] J.A.Z. Pieterse, G. Mul, I. Melián-Cabrera, R.W. van den Brink, Catal. Lett. 99 (2005) 41.
[9] I. Melián-Cabrera, S. Espinosa, F.J. García-Montelongo, F. Kapteijn, J.A. Moulijn, Chem. Commun. (2005) 1525–1527.
[10] D. Kaucký, Z. Sobalík, M. Schwarze, A. Vondrová, B. Wichterlová, J. Catal. 238 (2006) 293–300.
[11] J. Pérez-Ramírez, F. Kapteijn, G. Mul, J.A. Moulijn, Chem. Commun. 69 (2001) 3–694.
[12] G.D. Pirngruber, M. Luechinger, P.K. Roy, A. Cecchetto, P. Smirniotis, J. Catal. 224 (2004) 429–440.
[13] Q. Zhu, R.M. van Teeffelen, R.A. van Santen, E.J.M. Hensen, J. Catal. 221 (2004) 575–583.
[14] J. Pérez-Ramírez, J.C. Groen, A. Brückner, M.S. Kumar, U. Bentrup, M.N. Debbagh, L.A. Villaescusa, J. Catal. 232 (2005) 318–334.
[15] I. Melián-Cabrera, S. Espinosa, C. Mentruit, F. Kapteijn, J.A. Moulijn, Catal. Commun. 7 (2006) 100–103.
[16] I. Melián-Cabrera, S. Espinosa, J.C. Groen, B. v/d Linden, F. Kapteijn, J.A. Moulijn, J. Catal. 238 (2006) 250–259.
[17] K. Sun, H. Xia, E. Hensen, R. van Santen, C. Li, J. Catal. 238 (2006) 186–195.
[18] P.K. Roy, R. Prins, G.D. Pirngruber, Appl. Catal. B: Environ. 80 (2008) 226–236.
[19] G. Mul, M.W. Zandbergen, F. Kapteijn, J.A. Moulijn, J. Perez-Ramırez, Catal. Lett. 93 (2004) 113–120.
[20] I. Melián-Cabrera, F. Kapteijn, J.A. Moulijn, Chem. Commun. (2005) 2178–2180.
[21] J.A.Z. Pieterse, G.D. Pirngruber, J.A. van Bokhoven, S. Boneveld, Appl. Catal. B: Environ. 71 (2007) 16–22.
[22] B. Chen, N. Liu, X. Liu, R. Zhang, Y. Li, Y. Li, X. Sun, Catal. Today 175 (2011) 245–255.
[23] N. Liu, R. Zhang, B. Chen, Y. Li, Y. Li, J. Catal. 294 (2012) 99–112.
[24] M. Rutkowska, L. Chmielarz, D. Macina, Z. Piwowarska, B. Dudek, A. Adamski, S. Witkowski, Z. Sojka, L. Obalová, C.J. Van Oers, P. Cool, Appl. Catal. B: Environ. 146 (2014) 112–122.
[25] J.K. Lee, Y.J. Kim, H. Lee, S.H. Kim, S.J. Cho, I. Nam, S.B. Hong, J. Catal. 284 (2011) 23–33.
[26] K. Jisa, J. Novakova, M. Schwarze, A. Vondrova, S. Sklenak, Z. Sobalik, J. Catal. 262 (2009) 27–34.
[27] S. Sklenak, P.C. Andrikopoulos, B. Boekfa, B. Jansang, J. Nováková, L. Benco, T. Bucko, J. Hafner, J. Ddeek, Z. Sobalík, J. Catal. 272 (2010) 262–274.
[28] R. Zhang, N. Liu, Z. Lei, B. Chen, Chem. Rev. 116 (2016) 3658–3721.
[29] J. Pérez-Ramírez, G. Mul, F. Kapteijn, J.A. Moulijn, A.R. Overweg, A. Doménech, A. Ribera, I.W.C.E. Arends, J. Catal. 207 (2002) 113–126.
[30] E.J.M. Hensen, Q. Zhu, R.A. van Santen, J. Catal. 220 (2003) 260–264.
[31] E.J.M. Hensen, Q. Zhu, R.A.J. Janssen, P.C.M.M. Magusin, P.J. Kooyman, R.A. van Santen, J. Catal. 233 (2005) 123–135.
[32] E.J.M. Hensen, Q. Zhu, R.A. van Santen, J. Catal. 233 (2005) 136–146.
[33] E.J.M. Hensen, Q. Zhu, M.M.R.M. Hendrix, A.R. Overweg, P.J. Kooyman, M.V. Sychev, R.A. van Santen, J. Catal. 221 (2004) 560–574.
[34] Q. Zhu, R.M. van Teeffelen, R.A. van Santen, E.J.M. Hensen, J. Catal. 221 (2004) 575–583.

[35] J. Wang, H. Xia, X. Ju, Z. Feng, F. Fan, C. Li, J. Catal. 300 (2013) 251–259.
[36] J. Wang, H. Xia, X. Ju, Z. Feng, J. Wang, F. Fan, C. Li, J. Catal. 302 (2013) 91.
[37] H.K. Beyer, Dealumination techniques for zeolites, in: H.G. Karge, J. Weitkamp (Eds.), Molecular Sieves, Science and TechnologY. Post-Synthesis Modifications I, Springer-Verlag, Berlin, 2002, p. 203.
[38] S. Van Donk, A.H. Janssen, J.H. Bitter, K.P. de Jong, Catal. Rev. Sci. Technol. 45 (2003) 297–319.
[39] J. Perez-Ramirez, R.J. Berger, G. Mul, F. Kapteijn, J.A. Moulijn, Catal. Today 60 (2000) 93–109.
[40] F. Kapteijn, J. Rodriguez-Mirasol, J.A. Moulijn, Appl. Catal. B: Environ. 9 (1996) 25–64.
[41] F. Kapteijn, G. Mul, G. Marbán, J. Rodriguez-Mirasol, J.A. Moulijn, Stud. Surf. Sci. Catal. 101 (1996) 641–650.
[42] F. Kapteijn, G. Marbán, J. Rodriguez-Mirasol, J.A. Moulijn, J. Catal. 167 (1997) 256–265.
[43] M.F. de Lange, T.J.H. Vlugt, J. Gascon, F. Kapteijn, Microporous Mesoporous Mater. 200 (2014) 199–215.
[44] E.R.H. van Eck, J.A.Z. Pieterse, A.P.M. Kentgens, Solid State Nucl. Mag. 39 (2011) 99–105.
[45] M. Müller, G. Harvey, R. Prins, Micropor 34 (2000) 281–290.
[46] L.C. de Ménorval, W. Buckermann, F. Figueras, F. Fajula, J. Phys. Chem. 100 (1996) 465–467.
[47] J.A. van Bokhoven, D.C. Koningsberger, P. Kunkeler, H. van Bekkum, A.P.M. Kentgens, J. Am. Chem. Soc. 122 (2000) 12842–12847.
[48] A.E.W. Beers, J.A. van Bokhoven, K.M. de Lathouder, F. Kapteijn, J.A. Moulijn, J. Catal. 218 (2003) 239–248.
[49] F. Deng, Y. Yue, C. Ye, J. Phys. Chem. B 102 (1998) 5252–5256.
[50] J. Pérez-Ramírez, F. Kapteijn, J.C. Groen, A. Doménech, G. Mul, J.A. Moulijn, J. Catal. 214 (2003) 33–45.
[51] A.H. Øygarden, J. Pérez-Ramírez, Appl. Catal. B: Environ. 65 (2006) 163–167.
[52] J. Pérez-Ramírez, F. Kapteijn, G. Mul, J.A. Moulijn, J. Catal. 208 (2002) 211–223.
[53] G. Mul, J. Perez-Ramirez, F. Kapteijn, J.A. Moulijn, Catal. Lett. 77 (2001) 7–13.
[54] L. Kiwi-Minsker, D.A. Bulushev, A. Renken, J. Catal. 219 (2003) 273–285.
[55] N. Hansen, A. Heyden, A.T. Bell, F.J. Keil, J. Catal. 248 (2007) 213–225.
[56] G. Li, E.A. Pidko, I.A.W. Filot, R.A. van Santen, C. Li, E.J.M. Hensen, J. Catal. 308 (2013) 386–397.
[57] P. Sazama, E. Tabor, P. Klein, B. Wichterlova, S. Sklenak, L. Mokrzycki, V. Pashkkova, M. Ogura, J. Dedecek, J. Catal. 333 (2016) 102–114.
[58] P. Arnoldy, J.A. Moulijn, J. Catal. 93 (1985) 38–54.